1-1-2004

Beam element verification for 3D elastic steel frame analysis

Lip H. Teh
University of Wollongong, lteh@uow.edu.au

Beam Element Verification for 3D Elastic Steel Frame Analysis

Lip H. Teh

L.Teh@civil.usyd.edu.au

Department of Civil Engineering, University of Sydney, Sydney, NSW 2006, Australia

Abstract

The paper describes the attributes that should be possessed by a benchmark example for verifying the beam elements used to carry out 3D linear buckling analysis and 3D second-order elastic analysis of steel frames. Based on the attributes described, the paper proposes a suite of benchmark examples selected from the literature. The necessary features of a beam element required to pass the proposed benchmark problems are given, and beam elements that possess these features are cited. The paper also explains the merits of linear buckling analysis examples, and provides a commentary on two well-known examples.

Keywords: 3D second-order analysis, beam element, benchmarking, buckling analysis, elastic instability, lateral buckling, large displacement analysis, nonlinear frame analysis, steel frames, thin-walled structures

1. Introduction

In the past decade, there has been more widespread use of 3D frame analysis programs in civil engineering design offices to determine the buckling loads and the member forces of steel framed structures. In most cases, the use of 3D analysis has been necessitated by the topology of the designed structure that does not permit the use of 2D analysis, such as in the case of a sports

stadium. More recently, however, 3D frame analyses have also been carried out on multi-storey multi-bay rectangular frames such as high-rise storage rack frames. The fact that this type of steel structure is generally composed of open sections rather than tubular sections, the latter normally used in space roof trusses and offshore structures, has important implications for the frame stability that are not generally well understood by practising engineers. In design practice, either linear buckling analysis or second-order elastic analysis is performed to assess the frame stability.

The elastic buckling behaviour and the second-order effects due to geometric non-linearity of steel plane frames are well understood and well documented in the literature [1-4]. Commercial frame analysis programs that can handle most or all of these two stability aspects of planar (2D) steel structures have also been available for many years. For the purpose of verifying a 2D beam element or a 2D frame analysis program, there are many well established and well defined benchmark examples [5-7]. However, neither situation is true for 3D beam elements or 3D frame analysis programs. Although 3D linear elastic analysis is a fairly straightforward extension of 2D analysis, at the member level there may be 3D couplings between axial, flexural and torsional deformation modes that control the buckling behaviour of open sections. The comment of Springfield [8] that few commercial frame analysis/design programs could deal with out-of-plane buckling of beams or beam-columns by other than empirical means is still largely true today, except for the more expensive general-purpose finite element analysis packages such as ADINA [9] and ABAQUS [10]. The comment is even more apt in the case of flexural-torsional buckling of a compression member, although there are specialised computer programs such as PRFELB [11] and ConSteel [12] that are capable of flexural-torsional buckling analysis. This is despite the fact that limit states involving 3D member buckling modes are a practical reality [13-15].

To the author's knowledge, hitherto there is not a unified source that defines and justifies benchmark examples for verifying a 3D beam element used in the analysis and design of steel frames. From the practical point of view, a basic test of a proposed beam element or computer analysis program is whether it is validated by well defined benchmark examples [16]. Although the use of benchmark examples may not always resolve complex theoretical questions such as those discussed by Teh & Clarke [17-18], a well defined benchmark example helps identify the shortcomings of an element and safeguards against the use of computer analysis programs that are not sufficiently accurate for their purposes.

This paper discusses the attributes that should be possessed by a benchmark example for verifying the beam elements used to carry out 3D linear buckling analysis and 3D second-order elastic analysis of steel frames. Following the description of the essential and the desirable attributes of a benchmark example, the merits of linear buckling analysis examples vis-à-vis geometrically nonlinear analysis examples are discussed. A suite of benchmark examples selected from the literature are then proposed. Examples involving non-prismatic members, local buckling or distortional buckling are not included. This paper also provides a commentary on two popular examples that have been used to verify 3D beam elements in the literature.

2. Essential and desirable attributes of a benchmark example for 3D beam elements

The essential and the desirable attributes of a benchmark example for verifying 3D second-order beam elements used to analyse steel frames are listed in the following. The first five attributes are essential, and the last two are desirable:

i. The example clearly exhibits a specific member characteristic (or characteristics) which is unique to 3D problems, such as flexural-torsional buckling and warping torsion.

ii. When a certain 3D beam element fails the example, the reason or reasons for its failure can be identified so that the element can be refined if desired. This is an important attribute as the 3D beam elements (or stability function based beam-columns) used in many commercial frame analysis programs are direct extensions of 2D beam elements.

iii. The manner in which the example should be analysed is clearly prescribed. A 3D beam element that does not properly account for flexural-torsional coupling may be able to detect the flexural-torsional buckling load of a structure if geometric imperfections corresponding to the buckling mode are introduced into the geometrically nonlinear analysis model. This issue is discussed in details in Sections 3 and 4.9.

iv. The example has an experimental validation. In the absence of experimental validation, the example should be validated by the classical beam-column theory or an alternative analysis method that, in turn, has been validated experimentally for a similar problem or a problem of a higher degree of complexity.

v. The example is sufficiently documented so that the computer modelling can be performed by independent parties.

vi. The tested characteristic represents a fundamental structural behaviour that may be encountered in practice.

vii. The example requires minimal modelling efforts and analysis time.

A suite of benchmark examples should cover a reasonably comprehensive range of 3D buckling modes and nonlinear responses of steel members under various combinations of loading and boundary conditions. Section 4 proposes such a suite of benchmark examples within the context of elastic analysis.

3. Linear buckling analysis examples vs geometrically nonlinear analysis examples

This section aims to point out the advantages of linear buckling analysis examples over geometrically nonlinear analysis ones in verifying the ability of a beam element to properly capture the 3D instability phenomena of steel frames. This section also explains why it is important that a beam element be able to detect structural instability without the use of geometric imperfections or load perturbations.

A geometrically nonlinear analysis may miss the lowest buckling mode of a structure even if the decomposed tangent stiffness matrix contains a negative pivot signifying instability [19]. This shortcoming is not due to the beam element, but is due to the load incrementation strategy used in the nonlinear analysis algorithm. In this case, it cannot be ascertained whether the element is able to detect the lowest buckling mode. On the other hand, in a linear buckling analysis, such an ability of the element is not masked by the shortcoming of the load incrementation strategy.

Conversely, if geometric imperfections or perturbation loads conducive to the bifurcation buckling mode are introduced to the model, the nonlinear analysis may detect the lowest buckling mode even though a linear buckling analysis using the same element fails to detect that mode. In analysing the cantilevered right-angle frame depicted in Fig. 1, Leung & Wong [20] used the 3D beam element described by Meek & Tan [21], which is a direct extension of the 2D beam element presented by Jennings [22] with the addition of uniform torsion. Such a 3D beam element has been shown by Teh & Clarke [24] to fail to predict the lateral (flexural-torsional) buckling load of the cantilevered right-angle frame in a linear buckling analysis. However, by introducing a small perturbation force at the tip to induce the well-known lateral buckling, Leung & Wong [20] were

able to simulate the lateral buckling in their geometrically nonlinear analysis, as shown in Fig. 2. In this case, the bifurcation problem dissolves into a normal large displacement problem, and there is no issue concerning the singularity of the tangent stiffness matrix at the bifurcation point.

However, the use of perturbation forces or geometric imperfections to detect the lowest buckling load in a geometrically nonlinear analysis is not always feasible without an eigenmode analysis of the structure tangent stiffness matrix. The appropriate mode is not always obvious or well-known, while random imperfections do not guarantee that the lowest buckling mode will always be detected. The space dome depicted in Fig. 3 has been analysed by many researchers, yet most of them did not detect its flexural-torsional buckling mode [18]. Leung & Wong [20], who detected the well-known flexural-torsional buckling mode of the cantilevered right-angle frame of Fig. 1 through the use of a perturbation force corresponding to that mode, did not model the little known flexural-torsional buckling mode of the space dome, which they also analysed. As is the case with many other researchers, Leung & Wong [20] traced the unstable primary path of the space dome beyond the bifurcation point. The primary and the secondary equilibrium paths are shown in Fig. 4.

There is no doubt that geometrically nonlinear analysis examples have an important role in verifying 3D beam elements, especially for problems involving significant pre-buckling deformations. However, in the context of steel frame analysis and design, more importance should be given to linear buckling analysis examples in verifying 3D beam elements than is the case in the literature. This contention also holds for inelastic beam elements as linear buckling analysis examples serve to isolate any fundamental flaws in the element formulation, which is distinct from the theory of plasticity.

4. Proposed benchmark examples

4.1 Flexural-torsional buckling of a centrally loaded, simply supported unequal angle column

A doubly-symmetric I-section column generally buckles in the flexural mode. This buckling mode is so well known that many practising structural engineers consider this buckling mode only in designing steel columns. Some steel structures standards such as AS 4100 [26] only account for the flexural buckling mode explicitly in their design rules specified for a compression member, although there is a provision for local buckling which coincides with torsional buckling for certain sections. The perception that compression members can buckle in the flexural mode only may be reinforced by the traditional use of 2D buckling analysis in designing steel frames. Although this perception is justified for most steel columns used in civil engineering structures, it is not valid for those with low torsional rigidities and significant shear-centre eccentricities.

In addition to the flexural buckling mode, a thin-walled open section column with a low torsional rigidity may buckle in the torsional mode under concentric compression due to the so-called Wagner effect [27]. The elastic torsional buckling load is

$$P_x = \frac{GJ + \pi^2 EC_w / L^2}{r^2} \tag{1}$$

in which G is the elastic shear modulus, J is the uniform (St. Venant) torsion constant, E is the Young's modulus, C_w is the warping constant, L is the length of the simply supported column (both ends are restrained against twisting but are free to warp), and r is the radius of gyration

$$r = \sqrt{\frac{I_y + I_z}{A} + {y_s}^2 + {z_s}^2} \tag{2}$$

in which I_y is the second moment of area about the minor axis, I_z is the second moment of area about the major axis, A is the cross-sectional area, y_s is the shear-centre eccentricity measured parallel to the minor axis, and z_s the shear-centre eccentricity measured parallel to the major axis.

For a section in which the shear-centre and the centroid do not coincide with each other, there is an interaction between the flexural and the torsional buckling modes under concentric compression, resulting in the flexural-torsional buckling mode [13, 28-29]. The flexural-torsional buckling load P_{xyz} is the solution to the cubic equation

$$\begin{aligned} &P_{xyz}^{\,3}\left(r^2 - y_s^{\,2} - z_s^{\,2}\right) - P_{xyz}^{\,2}\left\{\left(P_x + P_y + P_z\right)r^2 - P_y z_s^{\,2} - P_z y_s^{\,2}\right\} + \\ &P_{xyz}\, r^2\left(P_x P_y + P_x P_z + P_y P_z\right) - P_x P_y P_z r^2 = 0 \end{aligned} \tag{3}$$

in which P_y is the flexural buckling load about the minor axis and P_z is the flexural buckling load about the major axis.

An example of a column section that is subject to the flexural-torsional buckling mode is the unequal angle section depicted in Fig. 5. In practice, the warping constant C_w of an angle section is assumed to be zero. The classical buckling loads of this section are plotted against the variable lengths of the centrally loaded, simply supported column in Fig. 6. The appropriate way to verify a 3D beam element (or beam-column) against this example is to carry out a series of linear buckling analyses using variable lengths of the simply supported column, without introducing geometric imperfections into the models.

It can be shown that the oft-cited 3D beam element described by Meek & Tan [21], which is a direct extension of the 2D beam element presented by Jennings [22], only predicts the flexural buckling loads P_y about the minor axis over the whole range of the column lengths. This

beam element neglects the Wagner effect and therefore cannot detect the torsional buckling load P_x [24], let alone the flexural-torsional buckling load P_{xyz}. Such a beam element (or beam-column) is widely used in commercial 3D frame analysis programs.

The ability to detect the torsional buckling mode of an isolated column should not be confused with the ability to detect the torsional buckling mode of a column as part of a 3D framed structure. For instance, the beam element described by Meek & Tan [21] is able to detect the apparent torsional buckling mode of such columns. However, what is actually detected is the torsional buckling mode of the frame as a whole. The associated frame buckling load may be higher than the frame buckling load predicted using the element which accounts for the Wagner effect [15].

It can also be shown that the stability function based beam-columns such as that presented by Kassimali & Abbasnia [30] cannot detect the flexural-torsional buckling load P_{xyz} as it does not account for the coupling between axial, flexural and torsional deformation modes.

The cubic beam elements presented by Conci [31] and Lin & Hsiao [32] are able to predict the flexural-torsional buckling loads P_{xyz} plotted in Fig. 6 over the whole range of the column lengths, using two elements [4]. The necessary features of such a beam element are:

- account for the Wagner effect,
- account for the shear-centre eccentricities, and
- account for the interaction between axial, flexural and torsional deformation modes.

4.2 Flexural-torsional buckling of a centrally loaded, simply supported lipped angle column

The previous example involves an angle section which is assumed to have no torsional warping rigidity (C_w equal to zero). A 3D beam element that does not account for torsional warping may be able to predict the flexural-torsional buckling loads of such sections accurately. However, most open sections such as I-sections, channel sections, and lipped angle sections (see Fig. 7 for an example) possess significant torsional warping rigidities that may dominate the corresponding St. Venant torsion rigidities [13-15, 27-28, 33-34]. Although the steel members in most building frames are not subjected to primary torques, the inclusion of torsional warping in the beam element is important for the linear buckling analysis of a structure composed of such sections.

Wagner & Pretschner [27] conducted a series of laboratory tests on centrally loaded and simply supported (both ends are prevented from twisting but are free to warp) lipped equal angle section columns. Due to the lips, the torsional warping rigidity is significant for relatively short columns. The Young's modulus of the material is E = 72.5 GPa. The geometric properties of the mono-symmetric section are: $A = 56.5\,\text{mm}^2$, $I_z = 9550\,\text{mm}^4$, $I_y = 2750\,\text{mm}^4$, $GJ = 392\,\text{kNmm}^2$, $C_w = 60000\,\text{mm}^6$ and $z_s = 13.6\,\text{mm}$.

The classical flexural-torsional buckling load P_{xz} of a mono-symmetric column is

$$P_{xz} = \frac{\left(P_x + P_z\right) - \sqrt{\left(P_x + P_z\right)^2 - 4P_xP_z\left(I_y + I_z\right)/\left(Ar^2\right)}}{2\left(I_y + I_z\right)/\left(Ar^2\right)} \tag{4}$$

The classical solutions and the buckling loads obtained in the laboratory tests [27] are

plotted in Fig. 8. For this mono-symmetric section, the flexural-torsional buckling mode is so dominated by the torsional buckling mode that their buckling loads are practically the same.

The solution obtained by neglecting the warping constant C_w in Equation (1), denoted P_v, is also shown in the figure. It can be seen that, even though both ends of the simply supported column are free to warp, the flexural-torsional buckling loads of the shorter columns are significantly affected by the torsional warping rigidity. For a beam element to predict the flexural-torsional buckling loads of these columns accurately, the finite element formulation must account for torsional warping of the cross-section, in addition to the Wagner effect and shear-centre eccentricity. Such beam elements, which possess fourteen nodal degrees of freedom, have been presented by Conci [31] and Lin & Hsiao [32], among others.

4.3 Flexural-torsional buckling of a simply supported doubly-symmetric I-section beam-column

The first two examples involve columns that buckle in the flexural-torsional mode under concentric compression due to shear-centre eccentricity. For a doubly-symmetric section, there is no shear-centre eccentricity and therefore no interaction between the flexural and the torsional buckling modes under concentric compression. A doubly-symmetric I-section column generally buckles in the flexural mode about the minor axis. However, an I-section beam that is bent about the major axis may buckle in the flexural-torsional mode (often called lateral buckling).

The lateral buckling (uniform) moment of a simply supported doubly-symmetric I-section beam (both ends are restrained against twisting but are free to warp) is

$$M_{xy} = \sqrt{\frac{\pi^2 EI_y}{L^2}\left(GJ + \frac{\pi^2 EC_w}{L^2}\right)} \tag{5}$$

Under combined compression and bending, the lateral buckling moment decreases with increasing axial load. Likewise, the axial load at which lateral buckling takes place under a given bending moment about the major axis is naturally less than the Euler buckling load about the minor axis. Under a uniform bending moment M_z', the critical load of a centrally loaded and simply supported beam-column is

$$P_{xy} = \frac{\left(P_x + P_y\right) - \sqrt{\left(P_x + P_y\right)^2 - 4\left\{P_x P_y - M_z'^2 \, A \big/ \left(I_y + I_z\right)\right\}}}{2} \tag{6}$$

Figure 9 plots the critical loads P_{xy} of a 5-metre simply supported doubly-symmetric I-section beam-column having the following section properties: $A = 11400\,\text{mm}^2$, $I_z = 1.43\times10^8\,\text{mm}^4$, $I_y = 4.84\times10^7\,\text{mm}^4$, $J = 1.04\times10^6\,\text{mm}^4$ and $C_w = 7.13\times10^{11}\,\text{mm}^6$. The steel material properties are E = 200 GPa and G = 80 GPa. The critical loads are plotted against the uniform bending moments M_z', expressed as ratios of the lateral buckling moment M_{xy}.

The beam element described by Meek & Tan [21] is unable to predict the critical loads P_{xy} plotted in Fig. 9, for the simple reason that torsional warping is neglected in their formulation. On the other hand, although Kassimali & Abbasnia [30] include the warping constant in the torsional stiffness of their stability function based beam-column, their formulation cannot deal with a buckling problem where the member ends are free to warp due to the neglect of the warping degree of freedom.

A cubic beam element that is able to reproduce the results plotted in Fig. 9 can be found in the well-known textbook by McGuire et al. [34], as demonstrated in [14] for a similar problem.

At each node of this beam element, there are three translational degrees of freedom, three rotational degrees of freedom and one warping degree of freedom.

4.4 Flexural-torsional buckling of a doubly-symmetric I-section cantilever

The first three examples concern the flexural-torsional instability of a column or a beam-column under compression. Perhaps a better known form of flexural-torsional instability is the lateral buckling of a flexural member bent about the major axis, such as that of the doubly-symmetric I-section cantilever shown in Fig. 10.

The transverse shear force at the tip of the cantilever shown in Fig. 10 acts at the centroid of the cross-section. Beam elements such as those described by Conci [31] and McGuire et al. [34] are able to predict the lateral buckling load of this structure. However, in practice, the load may act on the top flange rather than at the centroid (more precisely, the centre of twist). In such a case, the lateral buckling load may be significantly reduced due to the additional torque sympathetic to the lateral buckling mode [13, 36]. This reduction cannot be predicted by the 3D beam elements described by Conci [31] and McGuire et al. [34] since load eccentricities are not considered in their formulations. Beam elements that account for load eccentricities have been presented by Lin & Hsiao [37], Pi et al. [38] and Kim et al. [39], among others.

Anderson & Trahair [36] presented a series of laboratory test results of doubly-symmetric I-section cantilevers loaded at the centroid or at the top flange. The relevant material properties are: E = 65.1 GPa and G = 26.0 GPa. The geometric properties are: $A = 349\,\text{mm}^2$, $I_z = 3.20\times10^5\,\text{mm}^4$, $I_y = 1.64\times10^4\,\text{mm}^4$, $J = 886\,\text{mm}^4$ and $C_w = 2.14\times10^7\,\text{mm}^6$. The lateral buckling loads obtained in the laboratory tests, H_{test}, are shown in Table 1. Also shown in the last

column of the table are the buckling analysis results obtained by Lin & Hsiao [37] using their cubic beam element, which accounts for load eccentricities.

It can be seen from Table 1 that the inclusion of the effect of off-centre transverse shear loading is important in the design of a beam structure where the load can displace freely, such as in the case of a crane beam.

4.5 Flexural-torsional buckling of a tee cantilever

It is seen in Example 4.4 that off-centre transverse shear loading reduces the lateral buckling load of an I-section beam due to the additional torque sympathetic to the lateral buckling mode. This fact is not controversial as it is intuitively acceptable. However, it is less obvious that the lateral buckling load of a mono-symmetric I-section beam bent in the plane of section symmetry will be lower if the compression flange is the smaller flange rather than the larger flange. This phenomenon is closely related to the Wagner effect associated with the torsional buckling of a column.

Anderson & Trahair [36] presented a series of laboratory test results of tee cantilevers loaded in various ways, as depicted in Fig. 11. These results are useful in verifying the ability of a beam element to simulate the combined effects of section mono-symmetry and load eccentricity on the lateral buckling load of a flexural member. The relevant material properties of the tee section are: E = 65.1 GPa and G = 26.0 GPa. The section properties are: $A = 253\,\text{mm}^2$, $I_z = 1.45\times10^5\,\text{mm}^4$, $I_y = 8.22\times10^3\,\text{mm}^4$, $J = 571\,\text{mm}^4$ and $y_s = 22.4\,\text{mm}$. Table 2 lists the laboratory test results [36] and the finite element analysis results [40].

4.6 Post-buckling path of an I-section cantilever

The first five examples are buckling analysis examples which serve to verify the ability of a beam element to capture 3D instability modes at the member level. They do not verify the ability of the beam element to simulate geometrically nonlinear behaviour of steel members, which is important for advanced analysis of frames [4, 6, 8].

Woolcock & Trahair [35] presented the laboratory test results of an I-section cantilever including the elastic post-buckling paths. A gravity load was applied at the cantilever tip, at the centroid of the cross-section (see Fig. 10). The relevant material properties are: E = 64.1 GPa and G = 25.5 GPa. The section properties are: $A = 286\ \text{mm}^2$, $I_z = 2.35\times10^5\ \text{mm}^4$, $I_y = 5.58\times10^3\ \text{mm}^4$, $J = 681\text{mm}^4$ and $C_w = 7.11\times10^6\ \text{mm}^6$. The self-weight is 7.63×10^{-3} N/mm. The equilibrium path of the 3300 mm long cantilever measured in the laboratory test [35] is shown in Fig. 12. This equilibrium path was matched perfectly by Lin & Hsiao [37].

It is instructive to note that the post-buckling path of the cantilever is stable. It is therefore not feasible to assume in a nonlinear analysis that a beam immediately loses all its moment-carrying capacity when it buckles laterally, especially in the context of advanced analysis which seeks to predict the behaviour and strength of a frame accurately. The moment capacity of a compact beam bent about the major axis, whether elastic or inelastic, cannot be lower than its moment capacity about the minor axis.

4.7 Post-buckling path of a continuous beam structure

Example 4.6 involves a cantilever that is loaded at the centroid, as shown in Fig. 10. However, in practice, a beam load may be applied on the top flange of the I-section rather than at

the centroid. Woolcock & Trahair [41] conducted a series of laboratory tests on a two-span continuous beam where the loads were applied on the top flanges, as depicted in Fig. 13. The material and section properties are the same as in Example 4.6. The equilibrium paths obtained by Woolcock & Trahair [41] in their laboratory tests agree very well with their theoretical predictions. For the sake of clarity, only the theoretical paths are plotted in Fig. 14.

It can be seen from Fig. 14 that, as the member subjected to the load H_1 buckled laterally, the adjacent member also "buckled" laterally even though it was subjected to a load only half the lateral buckling load.

4.8 Geometrically nonlinear analysis of an angle cantilever under torsion

The first seven examples involve flexural-torsional instability of thin-walled open section members under compression or bending about the major axis. However, a higher order coupling between flexure and torsion also manifests in, say, the nonlinear response of an angle member loaded in torsion. This is despite the indication that the linear flexural buckling torque of an angle member is very high [42].

Gregory [43] conducted a laboratory test on an angle cantilever loaded with a torque at the tip. The material properties of the specimen are: E = 89.6 GPa and G = 33.4 GPa. The geometric properties of the equal angle section are: $A = 28.0\,\text{mm}^2$, $I_z = 773\,\text{mm}^4$, $I_y = 122\,\text{mm}^4$, $J = 8.62\,\text{mm}^4$, and $z_s = 5.36\,\text{mm}$. The cantilever is 178 mm long. The deflections of the shear-centre at the tip obtained in the laboratory test are shown in Fig. 15. These deflections were closely predicted by Attard [44] and Hsiao & Lin [40].

In order to trace the deflections of the shear-centre at the cantilever tip accurately, a beam element must account for the second-order bending effect of torsion in a section where the centroid and the shear-centre do not coincide with each other. This effect is related to the shortening effect of torsion (and therefore, to the Wagner effect) but appears to be neglected in many 3D second-order beam elements that account for shear-centre eccentricities [31, 39]. In order to account for this effect, the third order terms of the twist rate must be included in the element formulation [35, 40, 43-44]. The ability to model this effect is of a higher order than the ability to predict the flexural buckling of a torsion member [42].

4.9 Cantilevered right-angle frame

All the preceding examples involve a single member or a two-span beam. For such problems, the intricate issue concerning the rotational behaviour of nodal moments in space and its implication on flexural-torsional buckling analysis does not arise [17-18, 23-24, 34]. The issue only arises in a framed structure in which the members are connected non-collinearly, such as the cantilevered right-angle frame depicted in Fig. 1.

Spillers et al. [45] conducted a laboratory test on a structure similar to that depicted in Fig. 1. Owing to the impractical dimensions of the original structure described by Argyris et al. [23], the material and section properties used in the laboratory test were modified to: E = 74.5 GPa, G = 27.6 GPa, $I_z = 4162\ \text{mm}^4$, $I_y = 59.9\ \text{mm}^4$, and $J = 240\ \text{mm}^4$. The centroidal length of the clamped member is 270 mm, and that of the loaded member is 267 mm. The lateral buckling load was found in the laboratory test to be approximately 110 N.

The beam elements described by Meek & Tan [21] and Conci [31], and the stability function based beam-column described by Kassimali & Abbasnia [30] are unable to predict the

lateral buckling load of the cantilevered right-angle frame in a linear buckling analysis. The reason is that the rotational behaviour of the nodal moments of the beam element in space has not been properly taken into account in the geometric stiffness matrix [18, 24]. This shortcoming cannot be remedied by the use of more elements per member.

If a geometric imperfection or a perturbation force corresponding to the lateral buckling mode of the angle frame is used in the geometrically nonlinear analysis, then the beam element or beam-column described by Meek & Tan [21] and Kassimali & Abbasnia [30] will be able to predict the lateral buckling load accurately provided a sufficient number of elements are used. In this case, the bifurcation problem dissolves into a normal large displacement problem, and there is no issue concerning the singularity of the tangent stiffness matrix at the bifurcation point.

Alternatively, in order to predict the lateral buckling load and mode of the cantilevered right-angle frame in a linear buckling analysis, their geometric stiffness matrices need only a simple modification to account for the rotational behaviour of the nodal moments in space [24]. The inclusion of the proper rotational behaviour of the nodal moments results in an asymmetric tangent stiffness matrix [18, 24, 40, 45-48]. However, the tangent stiffness matrix may be symmetrised as the asymmetric part vanishes at equilibrium (which also means that it is irrelevant to a linear buckling analysis), resulting in much less computational efforts and memory requirement [18, 24, 48-49]. The ability to predict the buckling mode from the singularity of the structure tangent stiffness matrix without the use of geometric imperfections or perturbation forces is important as the geometric imperfections or perturbation forces conducive to the lowest buckling mode are not always apparent, while random imperfections are not a fool-proof means.

5. Well-known examples

5.1 Hexagonal frame

The hexagonal frame depicted in Fig. 16 was tested by Griggs [50] and has been analysed by many researchers. The laboratory test was a valuable exercise in studying the behaviour of shallow space frames, and can be used as a debug example to verify nonlinear frame analysis programs. This type of space frames is also a useful vehicle for illustrating the more subtle aspects of structural analysis and design [51].

However, the hexagonal frame should not be mistaken as a rigorous benchmark example for verifying a newly proposed 3D beam element or beam-column. Due to the frame topology, the loading condition and the section symmetry, all the members behave essentially as planar (2D) beam-columns rather than spatial beam-columns. Furthermore, there is no 3D instability mode at the member level. The sloping members of the hexagonal frame behave in a manner similar to the Williams' toggle [52], which buckles in a snap-through mode in a 2D plane.

5.2 Curved cantilever

The curved cantilever shown in Fig. 17, first analysed by Bathe & Bolourchi [53], is perhaps the most popular example for verifying 3D nonlinear beam elements. It is recommended as a benchmark problem by NAFEMS (National Agency for Finite Element Methods and Standards, UK), and has been analysed as such by many computational mechanics researchers [54-58].

It can be seen from Table 3 that the predictions of the vertical deflection of the cantilever tip given by various beam elements are close to the original one given by Bathe & Bolourchi

[53]. As such, this example provides a simple and effective means to check a computer program for nonlinear 3D frame analysis at the fundamental level.

For the purpose of demonstrating the rigor of a geometrically nonlinear 3D beam element, this example should be complemented by other examples. It can be seen from Table 3 that the tip deflection obtained by Crisfield [46] using the linear elastic, small strain beam element cast in the Co-rotational framework is very close to those obtained by Simo & Vu-Quoc [49] using the finite strain beam theory. Importantly, the two beam elements derived by Kouhia & Tuomala [25], which predict very different buckling loads for the cantilevered right-angle frame depicted in Fig. 1, predict similar deflections for the present curved cantilever.

6. Concluding remarks

The paper has described seven attributes that should be possessed by a benchmark example for verifying a 3D second-order beam element used in the analysis and design of steel frames. Based on these attributes, the paper proposes nine benchmark examples selected from the literature, all of which except for two have laboratory test results that were reasonably matched by theoretical predictions. The two linear buckling analysis examples which do not have experimental validation are based on the well established beam-column theory.

The member characteristics exhibited by the proposed benchmark examples are unique to 3D problems only, and cannot be captured by a number of 3D beam elements (or stability function based beam-columns) available in the literature. The necessary features that must be possessed by a beam element to pass the benchmark tests have been described in the paper.

It has been pointed out that the hexagonal frame widely used for verifying 3D second-order beam elements may not be an appropriate benchmark example.

Finally, although the examples proposed in the paper do not involve material inelasticity, it is suggested that a 3D second-order inelastic beam element should first pass the benchmark tests using these examples. Almost all the important 3D phenomena such as those associated with the Wagner effect, torsional warping, axial-torsional-flexural coupling, shear-centre eccentricity, load eccentricity, second-order bending effect of torsion, and rotational behaviour of nodal moments in space is not caused by material inelasticity, although they may interact with each other. The current theoretical impediment at the member level, if it still exists, to rigorous 3D advanced analysis of steel frames is not so much with the beam element formulation as with the theory of plasticity [59-60].

Acknowledgments

The author thanks Nick Trahair, Kuo-Mo Hsiao and Gregory Hancock for proof-reading the manuscript and suggesting improvements to it. Any opinions expressed in the paper are those of the writer, and do not necessarily reflect the views of the writer's colleagues. The writer also thanks Kim Pham for the prompt production of some figures used in the paper.

References

[1] Chen W. F., Lui E. M. Stability Design of Steel Frames, Boca Raton (FL): CRC Press, 1991.

[2] White D. W., Hajjar J. Application of second-order elastic analysis in LRFD: research to practice. Engrg. J., AISC, 1991; 28:133-148.

[3] Hancock G. J. Elastic method of analysis of rigid jointed frames including second order effects. Journal of the Australian Institute of Steel Construction, 1994; 28(3):10-18.

[4] Teh L. H. Cubic beam elements in practical analysis and design of steel frames. Engrg. Struct., 2001; 23:1243-1255.

[5] Hsiao, K. M., Hou, F. Y. Nonlinear finite element analysis of elastic frames. Comp. Struct., 1987; 26:693-701.

[6] Clarke M. J., Bridge R. Q., Hancock G. J., Trahair, N. S. Benchmarking and verification of second-order elastic and inelastic frame analysis programs. Plastic Hinge Based Methods for Advanced Analysis and Design of Steel Frames, D. W. White and W. F. Chen, eds., Structural Stability Research Council, Bethlehem, Pennsylvannia,1993; 245-274.

[7] Hancock G. J. Second order elastic analyses: Solution techniques and verification. Journal of the Australian Institute of Steel Construction, 1994; 28(3):19-25.

[8] Springfield J. Foreword. Plastic Hinge Based Methods for Advanced Analysis and Design of Steel Frames, D. W. White and W. F. Chen, eds., SSRC, Lehigh University, Pennsylvania, 1993; i-ii.

[9] ADINA R & D. Automatic Dynamic Incremental Nonlinear Analysis. Watertown, MA, 1995.

[10] Hibbit, Karlsson and Sorensen Inc. ABAQUS Version 6.2, Pawtucket, Rhode Island, 2001.

[11] Papangelis J. P., Trahair N. S., Hancock G. J. Elastic flexural-torsional buckling of structures by computer. Comp. Struct., 1998; 68:125-137.

[12] KESZ Ltd. ConSteel - Concurrent Steel Structural Design Program. User Manual, Budapest, Hungary, 2002.

[13] Trahair N. S. Flexural-Torsional Buckling of Structures, London: E&FN Spon, 1993.

[14] McGuire, W., Ziemian, R. Steel frame stability: Out-of-plane effects. Proc., First Int. Conf. Structural Stability and Dynamics, Taipei, Taiwan, 7-9 December 2000, 5-20.

[15] Teh L. H., Hancock G. J., Clarke M. J. Analysis and design of double-sided high-rise steel pallet rack frames. Accepted for publication in J. Struct. Eng., ASCE.

[16] Hajjar J. F. Advanced inelastic analysis for LRFD design: Guidelines for development and use. Plastic Hinge Based Methods for Advanced Analysis and Design of Steel Frames, D. W. White and W. F. Chen, eds., Structural Stability Research Council, Bethlehem, Pennsylvannia,1993; 191-210.

[17] Teh L. H., Clarke M. J. New definition of conservative internal moments in space frames. J. Engrg. Mech., 1997; 123:97-106.

[18] Teh L. H., Clarke M. J. Symmetry of tangent stiffness matrices of 3D elastic frame. J. Engrg. Mech., 1999; 125:248-251.

[19] Teh L. H., Clarke M. J. Tracing the secondary equilibrium paths of elastic framed structures. J. Engrg. Mech., 1999; 125: 1358-1364.

[20] Leung A. Y. T., Wong C. K. Symmetry reduction of structures for large rotations. Advances in Steel Structures, 2000; 3:81-102.

[21] Meek J. L., Tan H. S. Geometrically non-linear analysis of space frames by an incremental iterative technique. Comp. Meth. Appl. Mech. Engrg., 1984; 47:261-282.

[22] Jennings A. Frame analysis including change in geometry. J. Struct. Div., ASCE, 1968; 94:627-644.

[23] J. H. Argyris, O. Hilpert, G. A. Malejannakis, D. W. Scharpf. On the geometrical stiffnesses of a beam in space - a consistent V.W. approach. Comp. Meth. Appl. Mech. Engrg., 1979; 20:105-131

[24] Teh L. H., Clarke M. J. Co-rotational and Lagrangian formulations of elastic three-dimensional beam finite elements. J. Construct. Steel Res., 1998; 48:123-144.

[25] Kouhia R., Tuomala M. Static and dynamic analysis of space frames using simple Timoshenko type elements. Int. J. Numer. Meth. Engrg., 1993; 36:1189-1221.

[26] Standards Australia. Steel Structures, AS 4100-1998, Homebush, New South Wales, Australia, 1998.

[27] Wagner H., Pretschner W. Torsion and buckling of open sections, Technical Memorandum No. 784, National Advisory Committee for Aeronautics, Washington, DC, 1936.

[28] Timoshenko S. P., Gere J. M. Theory of Elastic Stability. 2nd ed. New York: McGraw-Hill, 1961.

[29] Chajes A., and Winter G. Torsional-flexural buckling of thin-walled members. *J. Struct. Div.*, ASCE, 1965; 91:103-124.

[30] Kassimali A., Abbasnia R. Large deformation analysis of elastic space frames. J. Struct. Engrg., 1991; 117: 2069-2087.

[31] Conci A. Large displacement analysis of thin-walled beams with generic open section. Int. J. Numer. Meth. Engrg., 1992; 33:2109-2127.

[32] Lin W. Y., Hsiao K. M. Co-rotational finite element formulation for thin-walled beam with generic open section. Proc., 5th Int. Conf. Space Structures, Guildford, U.K., 19-21 August 2002, G. A. R Parke and P. Disney, eds., Thomas Telford Publishing, London, 909-918.

[33] Vlasov, V. Z. Thin-Walled Elastic Beams, 2nd ed., Israel Program for Scientific Translation, Jerusalem, Israel, 1961.

[34] McGuire W., Gallagher R. H., Ziemian R. Matrix Structural Analysis. 2nd ed. New York: John Wiley & Sons, 2000.

[35] Woolcock S. T., Trahair N. S. Post-buckling behavior of determinate beams. J. Engrg. Mech. Div., ASCE, 1974; 100:151-171.

[36] Anderson J. M. , Trahair N. S. Stability of mono-symmetric beams and cantilevers. J. Struct. Div., ASCE, 1972; 98:269-286.

[37] Lin W. Y., Hsiao K. M. Co-rotational formulation for geometric nonlinear analysis of doubly symmetric thin-walled beams. Comp. Meth. Appl. Mech. Engrg., 2001; 190:6023-6052.

[38] Pi Y. L., Trahair N. S., Rajasekaran S. Energy equation for beam lateral buckling. J. Struct. Eng., 1992; 118:1462-1479.

[39] Kim M. Y., Chang S. P., Kim S. B. Spatial post-buckling analysis of non-symmetric thin-walled space frames. II: Geometrically nonlinear FE procedures. J. Engrg. Mech., 2001; 127:779-790.

[40] Hsiao K. M., Lin W. Y. A Co-rotational formulation for thin-walled beams with mono-symmetric open sections. Comp. Meth. Appl. Mech. Engrg., 2000; 190:1163-1185.

[41] Woolcock S. T., Trahair N. S. Post-buckling of redundant I-beams. J. Engrg. Mech. Div., ASCE, 1976; 102:293-312.

[42] Trahair N. S., Teh L. H. Second-order moments in torsion members. Engrg. Struct., 2001; 23:631-642.

[43] Gregory M. A nonlinear bending effect when certain unsymmetrical section are subjected to a pure torque. Australian J. Appl. Sci., 1960; 11:33-48.

[44] Attard M. The elastic flexural-torsional response of thin-walled open beams. PhD thesis, School of Civil Engineering, University of New South Wales, Kensington, Australia.

[45] Spillers W. R. Saadeghvaziri A., Luke A. An example of 3-dimensional frame buckling. Comp. Struct., 1993; 47:483-486.

[46] Crisfield M. A. A consistent co-rotational formulation for non-linear, three-dimensional beam elements. Comp. Meth. Appl. Mech. Engrg., 1990; 81:131-150.

[47] Teh L. H. Spatial rotation kinematics and flexural-torsional buckling. To be published in Special Issue on Stability, J. Engrg. Mech., ASCE, 2004.

[48] Nour-Omid B., Rankin C.C. Finite rotation analysis and consistent linearisation using projectors. Comp. Meth. Appl. Mech. Engrg., 1991; 93:353-384.

[49] Simo J. C., Vu-Quoc L. A three dimensional finite strain rod model, Part II: Computational aspects. Comp. Meth. Appl. Mech. Engrg., 1986; 58:79-115.

[50] Griggs, H. P. Experimental study of instability in elements of shallow space frames. Research Report, September 1966, Department of Civil Engineering, Massachusetts Institute of Technology, Cambridge, Massachusetts, 1966.

[51] Teh, L. H. Limitations of current design procedures for steel members in space frames. Proc. 2002 Stability and Ductility of Steel Structures, Budapest, Hungary, 26-28 September 2002, edited by M. Ivanyi, 315-322.

[52] Williams F. S. An approach to the nonlinear behaviour of the members of a rigid jointed plane framework with finite deflections. Quart. J. Mech. Appl. Math., 1964; 17:451-469.

[53] Bathe K. J., Bolourchi, S. Large displacement analysis of three-dimensional beam structures. Int. J. Numer. Meth. Engrg., 1979; 14:961-986.

[54] Rhim J., Lee S. W. A vectorial approach to computational modelling of beams undergoing finite rotations. Int. J. Numer. Meth. Engrg., 1998; 41:527-540.

[55] Cardona A., Geradin M. A beam finite element non-linear theory with finite rotations. Int. J. Numer. Meth. Engrg., 1988; 26:2403-2438.

[56] Dvorkin E. N., Onate E., Oliver J. On a non-linear formulation for curved Timoshenko beam elements considering large displacements/rotation increments. Int. J. Numer. Meth. Engrg., 1988; 26:1597-1613.

[57] Sandhu J. S., Stevens K. A., Davies G. A. O. A 3-D co-rotational, curved and twisted beam element. Comp. Struct., 1990; 35:69-79.

[58] Surana K. S., Sorem R. M. Geometrically non-linear formulation for three dimensional curved beam elements with large rotations. Int. J. Numer. Meth. Engrg., 1989; 28:43-73.

[59] McGuire W. Refining the plastic hinge concept. Proc., 1991 Annual Technical Session: Inelastic Behaviour and Design of Frames, Chicago, Illinois, 15-17 April 1991, SSRC, Lehigh University, Pennsylvania, 1-12.

[60] Teh L. H., Clarke M. J. Plastic-zone analysis of 3D steel frames using beam elements. J. Struct. Engrg., 1999; 125:1328-1337.

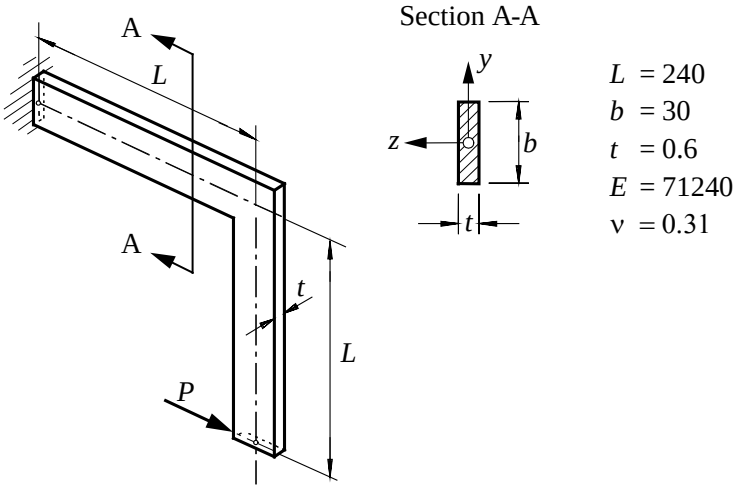

Fig. 1 Cantilevered right-angle frame subject to flexural-torsional buckling [23]

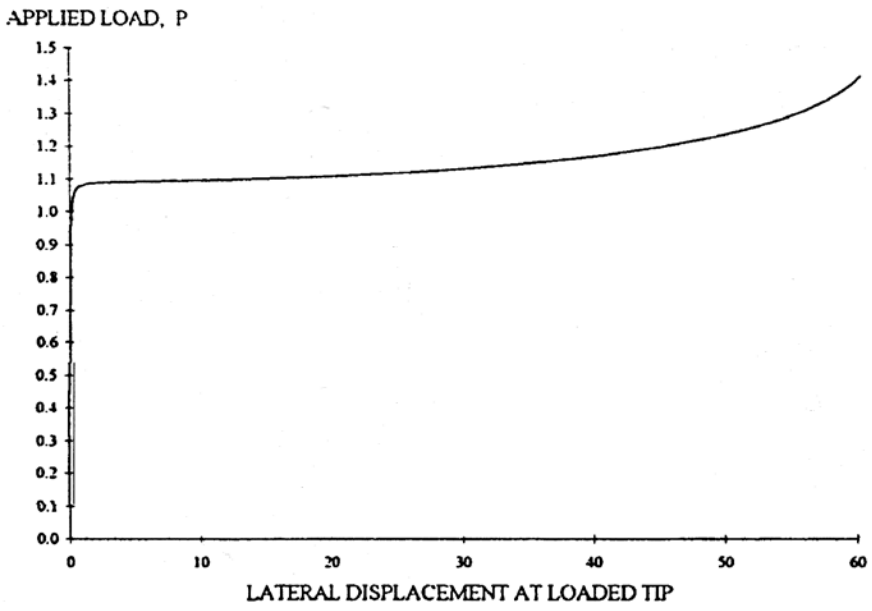

Fig. 2 Detecting “bifurcation” buckling by means of perturbation [20]

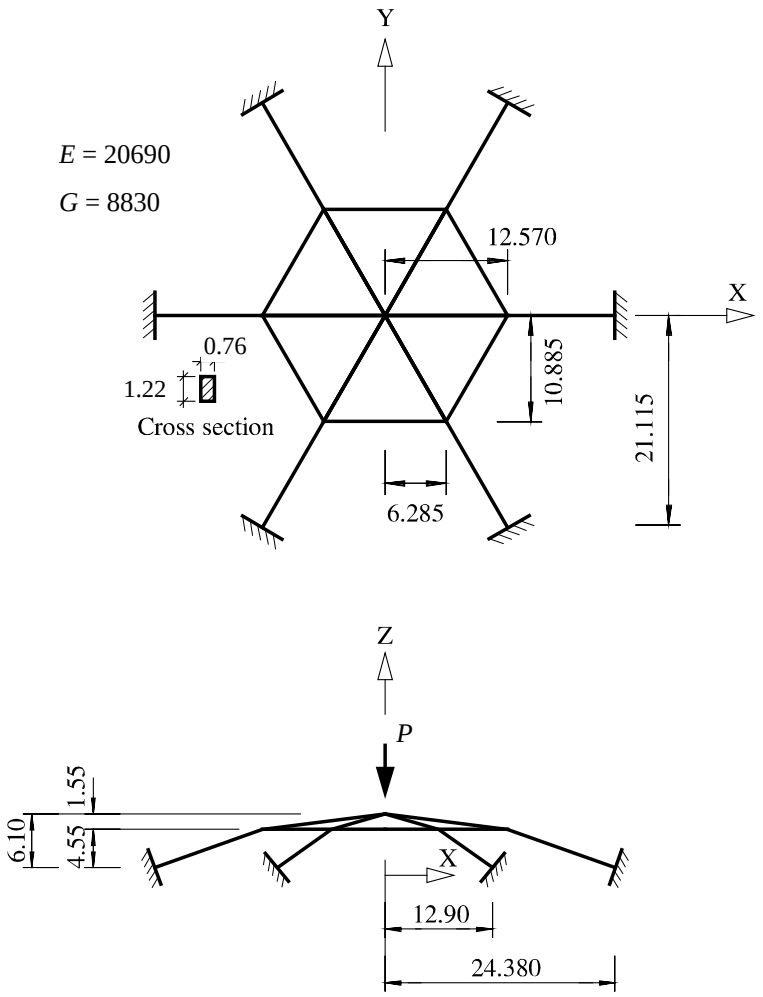

Fig. 3 Space dome subject to flexural-torsional buckling [25]

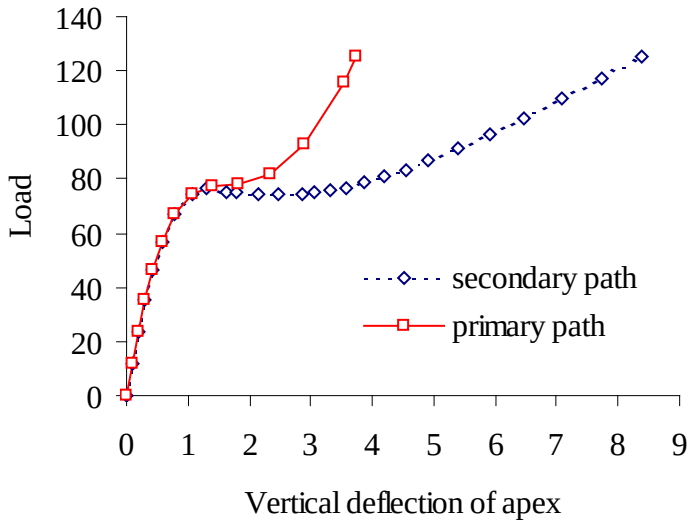

Fig. 4 Primary and secondary equilibrium paths of space dome

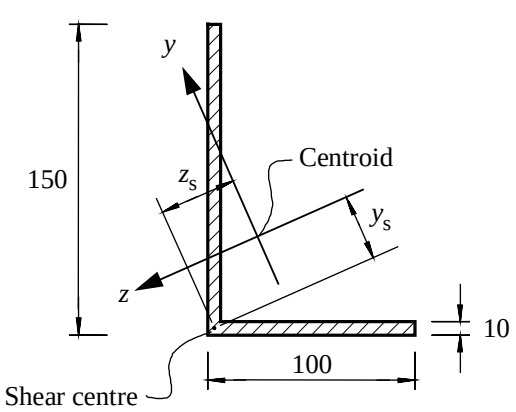

E = 200 GPa

G = 80 GPa

A = 2400 mm^2

I_z = 6.45 × 10^6 mm^4

I_y = 1.15 × 10^6 mm^4

J = 8.00 × 10^4 mm^4

y_s = 32.3 mm

z_s = 35.0 mm

Fig. 5 Unequal angle section

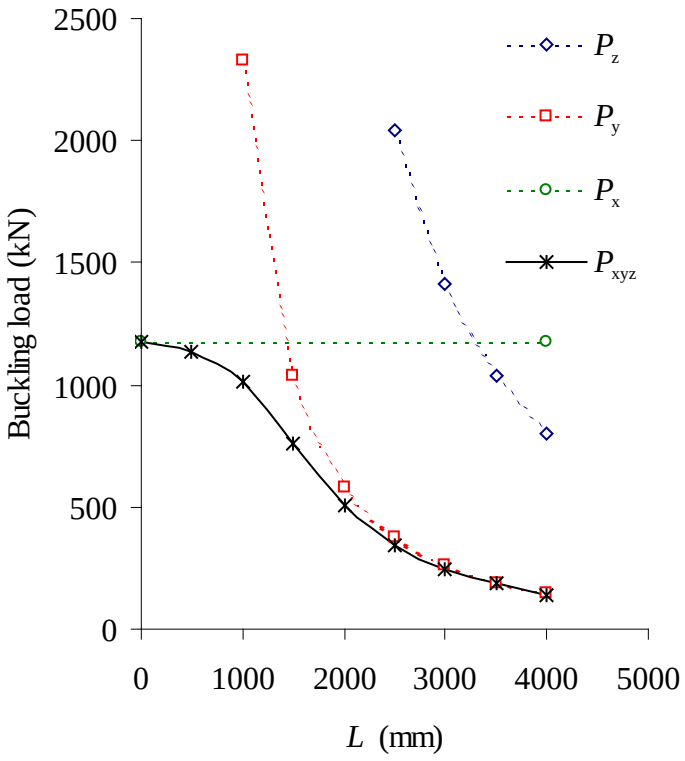

Fig. 6 Buckling loads of simply supported unequal angle columns

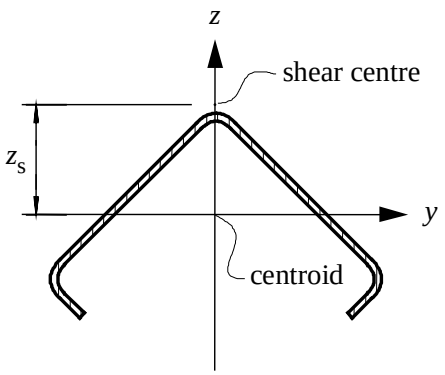

Fig. 7 Lipped angle section

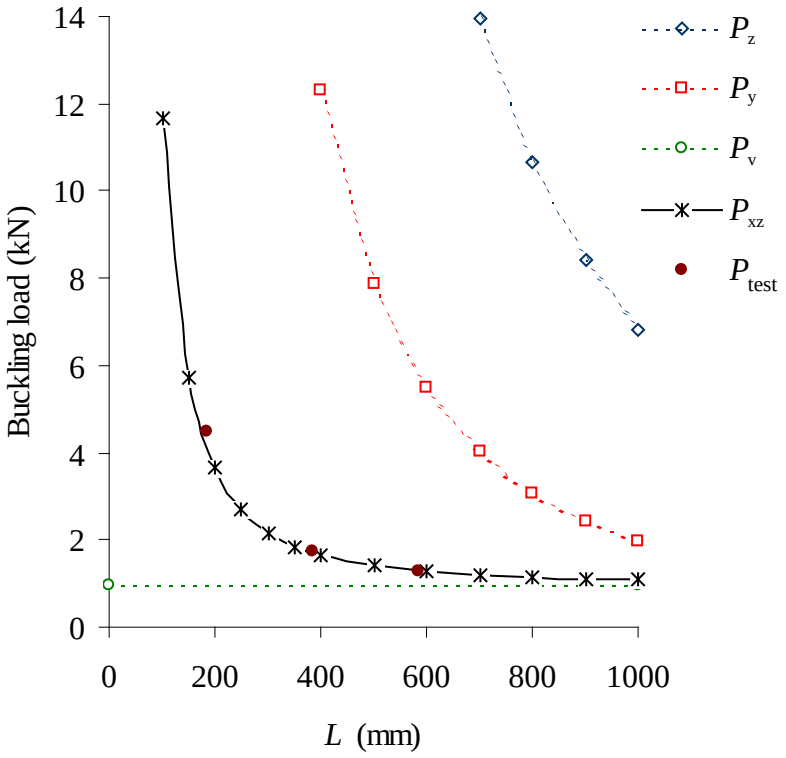

Fig. 8 Buckling loads of simply supported lipped equal angle columns

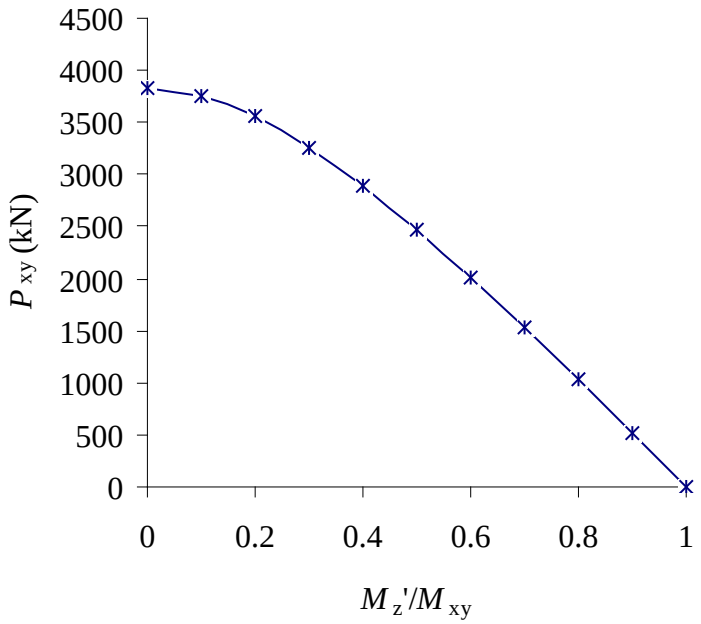

Fig. 9 Buckling loads of simply supported doubly-symmetric I-section beam-columns

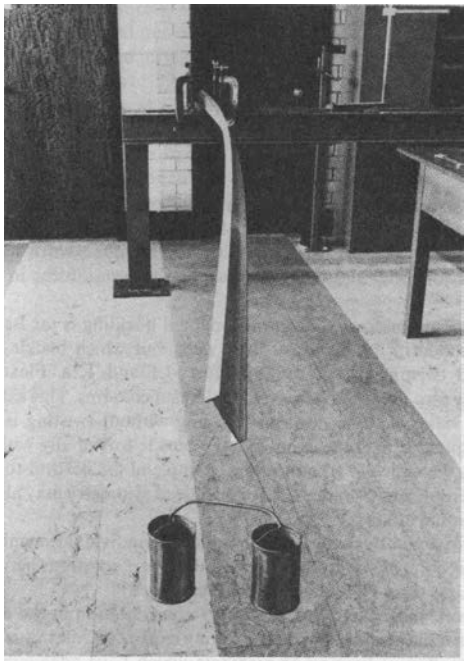

Fig. 10 Lateral buckling of a doubly-symmetric I-section cantilever [35]

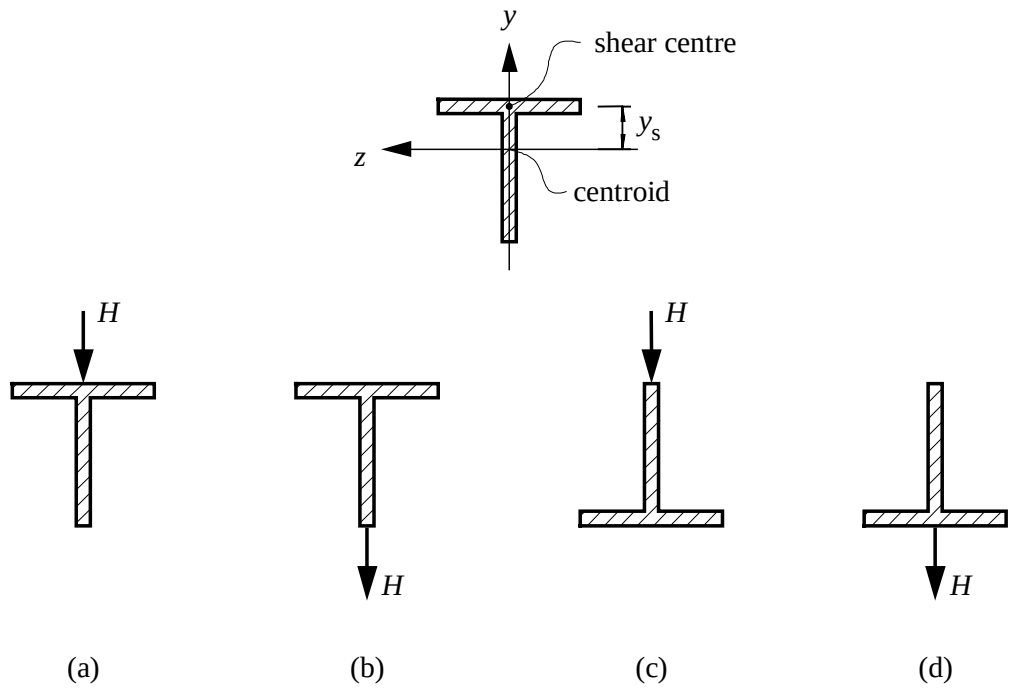

Fig. 11 Tee cantilevers loaded in various ways [36]

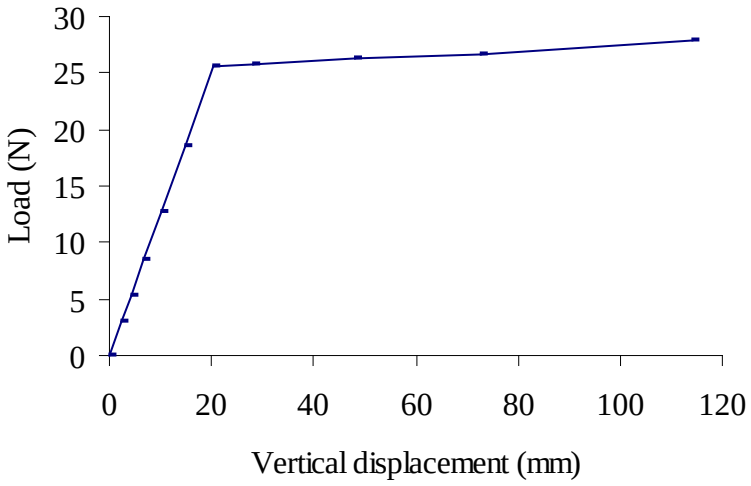

Fig. 12 Load-deflection graph of cantilever [35]

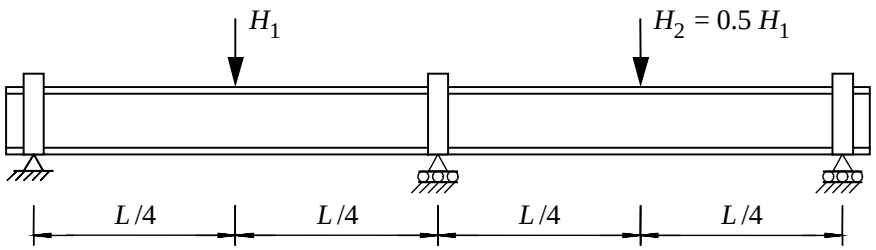

$L = 3658$ mm

Fig. 13 Two-span continuous beam with top-flange loadings [41]

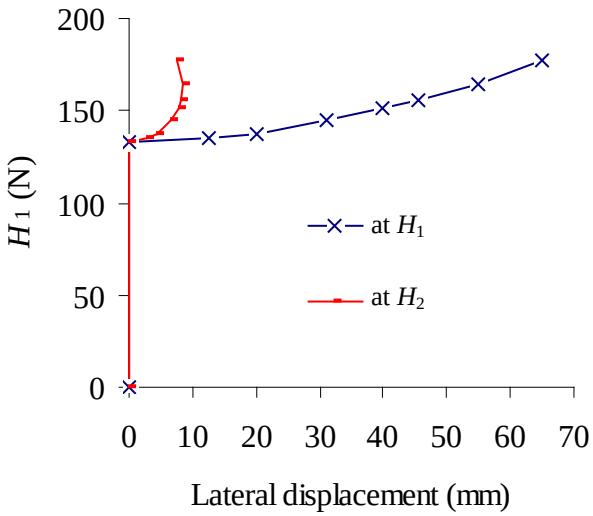

Fig. 14 Lateral displacements of two-span continuous beam [41]

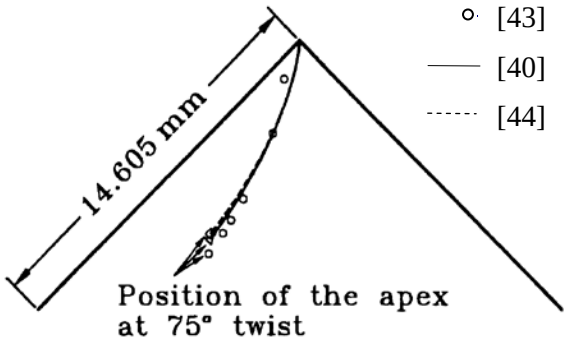

Fig. 15 Deflections of the angle’s shear-centre under clock-wise torque

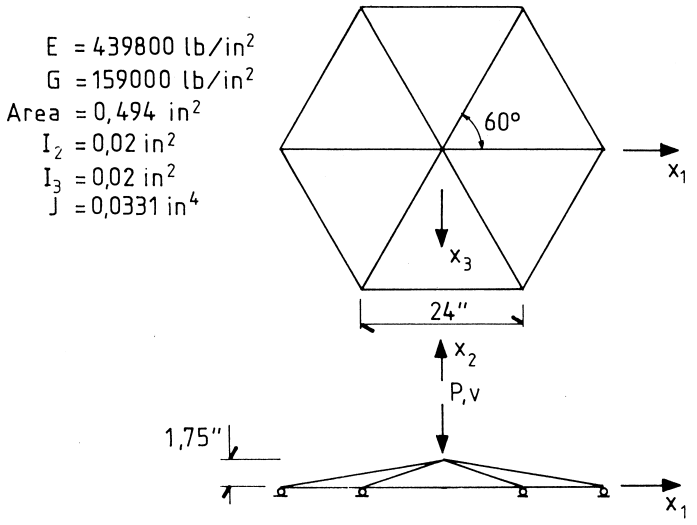

Fig. 16 Hexagonal frame [50]

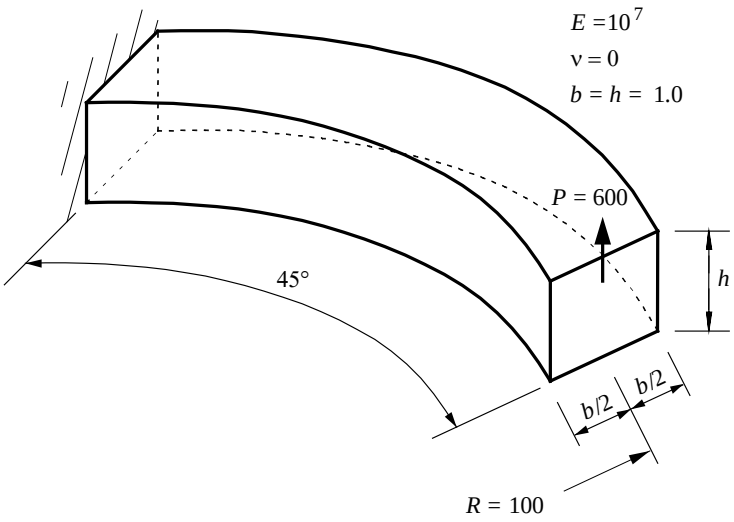

Fig. 17 Curved cantilever [53]

Table 1 Lateral buckling loads of doubly-symmetric I-section cantilevers

Length (mm)	*Location of Point Load*	H_{test} *(N) [36]*	H_{FEM} *(N) [37]*
1270	Centroid	597	614
	Top flange	406	408
1651	Centroid	323	331
	Top flange	257	242

Table 2 Lateral buckling loads of tee cantilevers

Length (mm)	*Transverse Load Arrangement*	H_{test} *(N) [36]*	H_{FEM} *(N) [40]*
1270	Fig. 11(a)	149	150
	Fig. 11(b)	168	175
	Fig. 11(c)	202	185
	Fig. 11(d)	374	375
1651	Fig. 11(a)	94	97
	Fig. 11(b)	108	112
	Fig. 11(c)	130	121
	Fig. 11(d)	191	200

Table 3 Analysis results of curved cantilever

	Vertical deflection of tip
[46]	53.7
[20]	53.6
[25a], [54], [55]	53.5
[49], [53]	53.4
[56], [57]	53.3
[25b]	53.2
[58]	53.0